

Application of the Nonlinear Tschauner-Hempel Equations to Satellite Relative Position Estimation and Control

Ranjan Vepa

(*Queen Mary, University of London, London E1 4NS*)

(E-mail: r.vepa@qmul.ac.uk)

In this paper we develop the nonlinear motion equations in terms of the true anomaly varying Tschauner–Hempel equations relative to a notional orbiting particle in a Keplerian orbit, relatively close to an orbiting primary satellite to estimate the position of a spacecraft. A second orbiting body in Earth orbit relatively close to the first is similarly modelled. The dynamic relative motion models of the satellite and the second orbiting body, both of which are modelled in terms of independent relative motion equations, include several perturbing effects, such as the asymmetry of the Earth gravitational field resulting in the Earth’s oblateness effect and the third body accelerations due to the Moon and the Sun. Linear control laws are synthesised for the primary satellite using the transition matrix so it can rendezvous with the second orbiting body. The control laws are then implemented using the state estimates obtained earlier to validate the feedback controller. Thus, we demonstrate the application of a Linear Quadratic Nonlinear Gaussian (LQNG) design methodology to the satellite rendezvous control design problem and validate it.

KEYWORDS

1. Nonlinear Estimation. 2. Optimal Control. 3. Relative Motion Dynamics. 4. Floquet Transition matrix.

Submitted: 17 April 2017. Accepted: 12 May 2017. First published online: 21 June 2017.

1. INTRODUCTION. The control of a satellite approaching another or any other orbiting body for purposes of engineering a smooth rendezvous is an important problem that has received considerable attention in the literature. Rendezvous and docking requires that the relative velocity and position of the chaser spacecraft be within stringent specified requirements for capture and berthing or docking with the help of a robotic arm as noted by the National Aerospace and Space Agency’s (NASA’s) mission operations directorate in NASA (2011), regarding several missions of the space shuttle. The linearized relative motion dynamics were first developed by Hill (1878) who was the first to linearize a set of equations to describe the motion of the moon relative to the Earth. Clohessy and Wiltshire (1960) published one of the most frequently used equations for relative satellite

motion for studying satellite rendezvous. Since the publication of the true anomaly-based TH equations by Tschauner and Hempel (1965), for the motion of one spacecraft relative to another, there have been a number of applications of these dynamical equations to spacecraft rendezvous and other related control problems. Coverstone-Carroll and Trussing (1993) were among the first to use the linearized true anomaly varying Tschauner-Hempel (TH) equations to design optimal rendezvous orbits. Yao et al. (2010) have considered the problem of orbit design for autonomous rendezvous based on relative orbit elements. Cui et al. (2011) have discussed the output feedback control of elliptical orbital rendezvous using solutions of the state-dependent Riccati differential equations. They used a linearized version of the TH equations for describing the relative motion of the approaching or chaser spacecraft. They have also reviewed the literature on the application of the linearized TH equations prior to the publication of their paper. Yazhong et al. (2014) have presented a survey of orbital dynamics and the control of space rendezvous. In his PhD, Felisiak (2015) dealt with the problem of the control of a spacecraft for performing a rendezvous manoeuvre while in an elliptical orbit by the methodology of model predictive control. Hartley et al. (2013), Leomanni et al. (2014) and Weiss et al. (2015) have applied model predictive control synthesis techniques to satellite rendezvous and proximity control problems.

Capó-Lugo and Bainum (2007) have presented active control schemes based on the linearized TH equations to maintain the separation distance constraints for a NASA benchmark tetrahedron satellite constellation. This a particular version of the formation control problem that involves the proximity control of two or more satellites, albeit a collision avoidance problem often involving the use of Artificial Potential Field (APF) to ensure that the satellites do not run into each other. Cho and Udwarda (2010) have provided an explicit solution to the full nonlinear problem for satellite formation-keeping. Capó-Lugo and Bainum (2011) have discussed the implementation of formation flying control for highly elliptical orbits. Condurache (2012) discusses spacecraft relative orbital motion, particularly focussing on obtaining closed form solutions for the motion. These are useful in synthesising analytic control laws to precisely control the relative motion. Nicholas (2013) considered the twin problems of attitude and formation control design and system simulation for a three-satellite CubeSat mission. Dwidar and Owis (2013) have adopted the linearized true anomaly varying Tschauner-Hempel equations, augmented to include the effect of J_2 , to study the optimal control of the relative motion of formation flying consisting of two spacecraft. Palacios et al. (2013) have studied the synthesis of an autonomous distributed Linear Quadratic Regulator (LQR) and APF-based control laws for swarms of CubeSats manoeuvring in eccentric orbits. Perez (2017) has applied relative motion dynamic models using curvilinear coordinate frames to derive and validate an angles-only initial relative orbit determination algorithm using three line-of-sight observations or six angle measurements.

In this paper we develop the nonlinear true anomaly varying TH equations relative to a notional orbiting particle, in a Keplerian orbit, relatively close to an orbiting primary satellite particularly in the presence of perturbing control accelerations. A second orbiting body in Earth orbit relatively close to the first is also modelled in terms of the nonlinear true anomaly varying TH equations. The linearized control laws are then synthesised based on these equations. The control inputs are scaled by similar scale factors used to scale the position coordinates in the original derivation by Tschauner and Hempel (1965). The dynamic relative motion models of the satellite and the other orbiting body, both of which are modelled in terms of independent relative motion equations, include several perturbing effects,

such as the asymmetry of the Earth gravitational field resulting in the Earth's oblateness effect and the third body accelerations due to the Moon and the Sun. The non-autonomous, nonlinear, true anomaly varying TH equations are used along with an Unscented Kalman Filter (UKF) to estimate the position of the primary spacecraft relative to the secondary orbiting body and the position of the secondary orbiting body relative to the notional body in Keplerian orbit. The performance of the state estimator is evaluated using an example of an Earth orbiting satellite at an altitude of over 1,200 km with debris in close proximity. It is shown that, with an additional post-processing filter, the estimates of position and velocity components of the primary satellite and the second orbiting body track the corresponding simulated position and velocity components within acceptable error magnitudes. Control laws are synthesised for the primary satellite using a finite horizon approach so it can come arbitrarily close to and rendezvous with the second orbiting body. The control laws are then implemented using the state estimates obtained earlier to validate the feedback controller using the TH equations. Thus, we demonstrate the application of a Linear Quadratic Non-linear Gaussian (LQNG) design methodology to the satellite rendezvous control design problem and validate it.

2. RELATIVE MOTION DYNAMICS. In the primary satellite's Local Vertical Local Horizontal (LVLH) frame, the position vector \mathbf{r}_o of the secondary orbiting body is given by the following,

$$\mathbf{r}_o = \mathbf{r} + \vec{\rho} = (r+x) i + yi + zk, \quad \mathbf{r}_o \cdot \mathbf{r}_o = (r+x)^2 + y^2 + z^2, \quad (1)$$

where \mathbf{r} is the position vector of the primary satellite, r is the magnitude of \mathbf{r} and $\vec{\rho} = xi + yi + zk$ is the position vector of the secondary orbiting body relative to the primary satellite. The angular velocity and acceleration of the LVLH frame, which is moving with the primary satellite, are given by $\omega = \dot{f} k = (h/hr^2)k$ and $\alpha = \dot{f} k = -(2\dot{r}/r) \omega = -(2\dot{r}/r) (h/r^2)k$ respectively, where f is the true anomaly and $h = |\mathbf{r} \times \dot{\mathbf{r}}|$ is the magnitude of the orbital angular momentum. Using Kepler's two body equations of motion for the primary satellite and for the secondary orbiting body both orbiting the Earth, $\ddot{\mathbf{r}} = -\mu_e/r^2$ and $\ddot{\mathbf{r}}_o = -\mu_e \mathbf{r}_o/r_o^3$ respectively, the vector equations of relative motion dynamics defining the temporal evolution of $\vec{\rho}$, under the influence of net perturbation acceleration vector \mathbf{a}_p are,

$$\frac{d^2 \vec{\rho}}{dt^2} = -\mu_e \left(\frac{(\mathbf{r} + \vec{\rho})^3}{|\mathbf{r} + \vec{\rho}|^3} - \frac{\mathbf{r}}{r^3} \right) + \mathbf{a}_p, \quad (2)$$

where $\mathbf{a}_p = \mathbf{a}_{po} - \mathbf{a}_{ps}$, \mathbf{a}_{ps} and \mathbf{a}_{po} are the perturbation accelerations due to the third body effects and Earth oblateness acting on the primary satellite and on the secondary orbiting body, which can be obtained from Vepa (2017). From kinematics, the equation of motion for the secondary orbiting body in the primary satellite's LVLH frame is given by the following:

$$\ddot{\mathbf{r}}_o = \ddot{\mathbf{r}} + \ddot{\vec{\rho}} + 2\omega \times \dot{\vec{\rho}} + \omega \times (\omega \times \vec{\rho}) + \alpha \times \vec{\rho}. \quad (3)$$

Thus, in component form we have,

$$\ddot{x} - 2\dot{f}\dot{y} - \dot{f}^2x - \ddot{f}y = a_{px} + (\mu_e/r^2) - \mu_e(r+x)/|\mathbf{r} + \vec{\rho}|^3, \tag{4a}$$

$$\ddot{y} + 2\dot{x}\dot{f} - \dot{f}^2y + \ddot{f}x = a_{py} - \mu_e y/|\mathbf{r} + \vec{\rho}|^3, \tag{4b}$$

$$\ddot{z} = a_{pz} - \mu_e z/|\mathbf{r} + \vec{\rho}|^3. \tag{4c}$$

In matrix notation, after including the linear terms of the right-hand sides, in the left-hand side of the equation,

$$\begin{aligned} \begin{bmatrix} \ddot{x} \\ \ddot{y} \\ \ddot{z} \end{bmatrix} + \dot{f} \begin{bmatrix} 0 & -2 & 0 \\ 2 & 0 & 0 \\ 0 & 0 & 0 \end{bmatrix} \begin{bmatrix} \dot{x} \\ \dot{y} \\ \dot{z} \end{bmatrix} + \begin{bmatrix} -\dot{f}^2 - 2(\mu_e/r^3) & -\ddot{f} & 0 \\ \ddot{f} & -\dot{f}^2 + (\mu_e/r^3) & 0 \\ 0 & 0 & (\mu_e/r^3) \end{bmatrix} \begin{bmatrix} x \\ y \\ z \end{bmatrix} \\ = \begin{bmatrix} a_{px} - (\mu_e(r+x)/|\mathbf{r} + \vec{\rho}|^3 - (\mu_e/r^2)(1 - 2x/r)) \\ a_{py} - (\mu_e y/|\mathbf{r} + \vec{\rho}|^3) + (\mu_e/r^2)(y/r) \\ a_{pz} - (\mu_e z/|\mathbf{r} + \vec{\rho}|^3) + (\mu_e/r^2)(z/r) \end{bmatrix} \end{aligned} \tag{5}$$

Ignoring the right-hand sides' results in the equations which are called the Linearized Equations of Relative Motion (LERM). Equations (5) are the Nonlinear Equations of Relative Motion (NERM), which can be expressed as,

$$\begin{aligned} \begin{bmatrix} \ddot{x} \\ \ddot{y} \\ \ddot{z} \end{bmatrix} + \dot{f} \begin{bmatrix} 0 & -2 & 0 \\ 2 & 0 & 0 \\ 0 & 0 & 0 \end{bmatrix} \begin{bmatrix} \dot{x} \\ \dot{y} \\ \dot{z} \end{bmatrix} + \begin{bmatrix} -\dot{f}^2 - 2(\mu_e/r^3) & -\ddot{f} & 0 \\ \ddot{f} & -\dot{f}^2 + (\mu_e/r^3) & 0 \\ 0 & 0 & (\mu_e/r^3) \end{bmatrix} \begin{bmatrix} x \\ y \\ z \end{bmatrix} \\ = \begin{bmatrix} a_{px} + \frac{\mu_e r}{r^3} \left(1 - 2\frac{x}{r} - \left(1 + \frac{x}{r} \right) \left(1 + 2\frac{x}{r} + \frac{x^2 + y^2 + z^2}{r^2} \right)^{-3/2} \right) \\ a_{py} + \frac{\mu_e y}{r^3} \left(1 - \left(1 + 2\frac{x}{r} + \frac{x^2 + y^2 + z^2}{r^2} \right)^{-3/2} \right) \\ a_{pz} + \frac{\mu_e z}{r^3} \left(1 - \left(1 + 2\frac{x}{r} + \frac{x^2 + y^2 + z^2}{r^2} \right)^{-3/2} \right) \end{bmatrix}. \end{aligned} \tag{6}$$

To obtain the Hill Clohessy Wiltshire (HCW) equations, we let $\dot{f} - n = \ddot{f} = 0$, $\dot{f}^2 = \mu_e/r^3 = n^2$, where n represents the mean rate of motion of the primary satellite or the mean motion. The system can be described by the state vector $\mathbf{x} = [x \ y \ z \ \dot{x} \ \dot{y} \ \dot{z}]^T$. In state-space form, the LERM are given by the equation, $\dot{\mathbf{x}} = \mathbf{A}(t)\mathbf{x}$, where

$$\mathbf{A}(t) = \begin{bmatrix} 0 & 0 & 0 & 1 & 0 & 0 \\ 0 & 0 & 0 & 0 & 1 & 0 \\ 0 & 0 & 0 & 0 & 0 & 1 \\ \dot{f}^2 + 2\mu_e/r^3 & \dot{f} & 0 & 0 & 2\dot{f} & 0 \\ -\ddot{f} & \dot{f}^2 - \mu_e/r^3 & 0 & -2\dot{f} & 0 & 0 \\ 0 & 0 & -\mu_e/r^3 & 0 & 0 & 0 \end{bmatrix}. \tag{7}$$

The matrix $\mathbf{A}(t)$ is time varying as r, \dot{f}, \ddot{f} vary with time. Thus $\mathbf{A}(t)$ is periodic with the period equal to $T = 2\pi/n$. The NERM may be expressed compactly as,

$$\frac{d^2}{dt^2} \begin{bmatrix} x \\ y \\ z \end{bmatrix} = -\dot{f}^2 \mathbf{K}_{lerm} \begin{bmatrix} x \\ y \\ z \end{bmatrix} - \dot{f} \mathbf{G}_{lerm} \frac{d}{dt} \begin{bmatrix} x \\ y \\ z \end{bmatrix} + \begin{bmatrix} \tilde{a}_{nx} \\ \tilde{a}_{ny} \\ \tilde{a}_{nz} \end{bmatrix}, \tag{8a}$$

where,

$$\mathbf{K}_{lerm} = \frac{1}{\dot{f}^2} \begin{bmatrix} -\dot{f}^2 - 2\frac{\mu_e}{r^3} & -\ddot{f} & 0 \\ \ddot{f} & -\dot{f}^2 + \frac{\mu_e}{r^3} & 0 \\ 0 & 0 & \frac{\mu_e}{r^3} \end{bmatrix}, \quad \mathbf{G}_{lerm} = \begin{bmatrix} 0 & -2 & 0 \\ 2 & 0 & 0 \\ 0 & 0 & 0 \end{bmatrix} \tag{8b}$$

and

$$\begin{bmatrix} \tilde{a}_{nx} \\ \tilde{a}_{ny} \\ \tilde{a}_{nz} \end{bmatrix} = \begin{bmatrix} a_{px} - \left(\mu_e (r+x) / |\mathbf{r} + \vec{\rho}|^3 - (\mu_e/r^2) (1 - 2x/r) \right) \\ a_{py} - \left(\mu_e y / |\mathbf{r} + \vec{\rho}|^3 \right) + (\mu_e/r^2) (y/r) \\ a_{pz} - \left(\mu_e z / |\mathbf{r} + \vec{\rho}|^3 \right) + (\mu_e/r^2) (z/r) \end{bmatrix}. \tag{8c}$$

3. DERIVATION OF THE NONLINEAR CONTROLLED TH EQUATIONS. The TH equations are obtained by using the true anomaly f as the independent variable. Moreover, Tschauner and Hempel (1965) also apply a coordinate scaling prior to transforming the equations. The scaled state variable \tilde{x} is related to the original state by the relation, $\tilde{x} = (1 + e \cos f) x$. Further,

$$d/df = d/\dot{f} dt = (r^2/h) d/dt, \quad r = p / (1 + e \cos f), \tag{9}$$

where p is the semi-latus rectum and $h = \sqrt{\mu p}$. It follows that,

$$\frac{d\tilde{x}}{df} = -ex \sin f + (1 + e \cos f) \frac{dx}{df}, \quad \frac{dx}{df} = \frac{r^2}{h} \frac{dx}{dt} = \frac{p^2}{h(1 + e \cos f)^2} \frac{dx}{dt}. \tag{10}$$

Thus,

$$\frac{d\tilde{x}}{df} = -ex \sin f + \frac{p^2}{h(1 + e \cos f)} \frac{dx}{dt}, \tag{11}$$

It follows that,

$$\begin{bmatrix} \tilde{x} \\ \tilde{y} \\ \tilde{z} \end{bmatrix} = (1 + e \cos f) \begin{bmatrix} x \\ y \\ z \end{bmatrix}, \quad \frac{d}{df} \begin{bmatrix} \tilde{x} \\ \tilde{y} \\ \tilde{z} \end{bmatrix} = -e \sin f \begin{bmatrix} x \\ y \\ z \end{bmatrix} + \frac{p^2}{h(1 + e \cos f)} \frac{d}{dt} \begin{bmatrix} x \\ y \\ z \end{bmatrix}. \tag{12}$$

The inverse transformations are,

$$\begin{bmatrix} x \\ y \\ z \end{bmatrix} = \frac{1}{(1 + e \cos f)} \begin{bmatrix} \tilde{x} \\ \tilde{y} \\ \tilde{z} \end{bmatrix}, \quad \frac{d}{df} \begin{bmatrix} x \\ y \\ z \end{bmatrix} = \frac{p^2}{h(1 + e \cos f)^2} \frac{d}{dt} \begin{bmatrix} x \\ y \\ z \end{bmatrix}. \tag{13}$$

Thus

$$\frac{(1 + e \cos f)}{f} \frac{d}{dt} \begin{bmatrix} x \\ y \\ z \end{bmatrix} = \frac{d}{df} \begin{bmatrix} \tilde{x} \\ \tilde{y} \\ \tilde{z} \end{bmatrix} + \frac{e \sin f}{(1 + e \cos f)} \begin{bmatrix} \tilde{x} \\ \tilde{y} \\ \tilde{z} \end{bmatrix}. \tag{14}$$

Consequently, we obtain,

$$\frac{d}{df} \begin{bmatrix} x \\ y \\ z \end{bmatrix} = \frac{e \sin f}{(1 + e \cos f)^2} \begin{bmatrix} \tilde{x} \\ \tilde{y} \\ \tilde{z} \end{bmatrix} + \frac{1}{(1 + e \cos f)} \frac{d}{df} \begin{bmatrix} \tilde{x} \\ \tilde{y} \\ \tilde{z} \end{bmatrix}. \tag{15}$$

Thus, the transformation relating the state vector takes the form, $\tilde{\mathbf{x}} = \mathbf{T}\mathbf{x}$,

$$\tilde{\mathbf{x}} = [\tilde{x} \ \tilde{y} \ \tilde{z} \ \tilde{x}' \ \tilde{y}' \ \tilde{z}']^T, \mathbf{x} = [x \ y \ z \ \dot{x} \ \dot{y} \ \dot{z}]^T, \tag{16}$$

$$\mathbf{T} = \begin{bmatrix} (1 + e \cos f) \mathbf{I} & \mathbf{0} \\ -(e \sin f) \mathbf{I} & \frac{p^2}{h(1 + e \cos f)} \mathbf{I} \end{bmatrix}, \mathbf{T}^{-1} = \begin{bmatrix} \frac{1}{(1 + e \cos f)} \mathbf{I} & \mathbf{0} \\ \frac{h(e \sin f)}{p^2} \mathbf{I} & \frac{h(1 + e \cos f)}{p^2} \mathbf{I} \end{bmatrix}. \tag{17}$$

Furthermore,

$$\frac{d^2}{df^2} \begin{bmatrix} \tilde{x} \\ \tilde{y} \\ \tilde{z} \end{bmatrix} = -e \cos f \begin{bmatrix} x \\ y \\ z \end{bmatrix} + \frac{p^2}{h(1 + e \cos f)} \frac{d}{dt} \frac{d}{df} \begin{bmatrix} x \\ y \\ z \end{bmatrix}. \tag{18}$$

Hence,

$$\frac{d^2}{df^2} \begin{bmatrix} \tilde{x} \\ \tilde{y} \\ \tilde{z} \end{bmatrix} = -e \cos f \begin{bmatrix} x \\ y \\ z \end{bmatrix} + \frac{1 + e \cos f}{f^2} \frac{d^2}{dt^2} \begin{bmatrix} x \\ y \\ z \end{bmatrix}. \tag{19}$$

It follows that,

$$\frac{d^2}{df^2} \begin{bmatrix} \tilde{x} \\ \tilde{y} \\ \tilde{z} \end{bmatrix} = - \begin{bmatrix} \tilde{x} \\ \tilde{y} \\ \tilde{z} \end{bmatrix} + \frac{1}{1 + e \cos f} \begin{bmatrix} \tilde{x} \\ \tilde{y} \\ \tilde{z} \end{bmatrix} + \frac{1 + e \cos f}{f^2} \frac{d^2}{dt^2} \begin{bmatrix} x \\ y \\ z \end{bmatrix}. \tag{20}$$

Noting that $p/r = (1 + e \cos f)$, from Equation (8a) we have,

$$\begin{aligned} \frac{d^2}{df^2} \begin{bmatrix} \tilde{x} \\ \tilde{y} \\ \tilde{z} \end{bmatrix} &= - \begin{bmatrix} \tilde{x} \\ \tilde{y} \\ \tilde{z} \end{bmatrix} + \frac{r}{p} \begin{bmatrix} \tilde{x} \\ \tilde{y} \\ \tilde{z} \end{bmatrix} - \mathbf{K}_{lerm} \begin{bmatrix} \tilde{x} \\ \tilde{y} \\ \tilde{z} \end{bmatrix} - \mathbf{G}_{lerm} \left\{ \frac{d}{df} \begin{bmatrix} \tilde{x} \\ \tilde{y} \\ \tilde{z} \end{bmatrix} + \frac{re \sin f}{p} \begin{bmatrix} \tilde{x} \\ \tilde{y} \\ \tilde{z} \end{bmatrix} \right\} \\ &+ \frac{r}{pf^2} \begin{bmatrix} \tilde{a}_{nx} \\ \tilde{a}_{ny} \\ \tilde{a}_{nz} \end{bmatrix}. \end{aligned} \tag{21}$$

Thus,

$$\begin{aligned} \frac{d^2}{df^2} \begin{bmatrix} \tilde{x} \\ \tilde{y} \\ \tilde{z} \end{bmatrix} &= -(\mathbf{K}_{lerm} + \mathbf{I}) \begin{bmatrix} \tilde{x} \\ \tilde{y} \\ \tilde{z} \end{bmatrix} - \frac{re \sin f}{p} \mathbf{G}_{lerm} \begin{bmatrix} \tilde{x} \\ \tilde{y} \\ \tilde{z} \end{bmatrix} + \frac{\mathbf{I}r}{p} \begin{bmatrix} \tilde{x} \\ \tilde{y} \\ \tilde{z} \end{bmatrix} - \mathbf{G}_{lerm} \frac{d}{df} \begin{bmatrix} \tilde{x} \\ \tilde{y} \\ \tilde{z} \end{bmatrix} \\ &+ \frac{r}{p\dot{f}^2} \begin{bmatrix} \tilde{a}_{nx} \\ \tilde{a}_{ny} \\ \tilde{a}_{nz} \end{bmatrix}. \end{aligned} \quad (22)$$

But,

$$\begin{aligned} &\mathbf{K}_{lerm} + \mathbf{I} + \frac{r(e \sin f)}{p} \mathbf{G}_{lerm} - \frac{r}{p} \mathbf{I} \\ &= \left(\frac{1}{\dot{f}} - 1 \right) \frac{2re \sin f}{p} \begin{bmatrix} 0 & 2 & 0 \\ -2 & 0 & 0 \\ 0 & 0 & 0 \end{bmatrix} + \frac{r}{p} \begin{bmatrix} -2 & -1 & 0 \\ 0 & 1 & -1 \\ 0 & 0 & 1 + 1 + e \cos f \end{bmatrix}. \end{aligned} \quad (23)$$

Hence,

$$\begin{aligned} &\mathbf{K}_{lerm} + \mathbf{I} + \frac{(e \sin f)}{(1 + e \cos f)} \mathbf{G}_{lerm} - \frac{1}{1 + e \cos f} \mathbf{I} \\ &= \left(\frac{p^2}{h(1 + e \cos f)^2} - 1 \right) \frac{2e \sin f}{(1 + e \cos f)} \begin{bmatrix} 0 & 2 & 0 \\ -2 & 0 & 0 \\ 0 & 0 & 0 \end{bmatrix} \\ &+ \frac{1}{(1 + e \cos f)} \begin{bmatrix} -3 & 0 & 0 \\ 0 & 0 & 0 \\ 0 & 0 & 2 + e \cos f \end{bmatrix}. \end{aligned} \quad (24)$$

Hence if we let,

$$\begin{aligned} \tilde{\mathbf{K}}_{lerm} &= \frac{1}{(1 + e \cos f)} \left\{ \begin{bmatrix} -3 & 0 & 0 \\ 0 & 0 & 0 \\ 0 & 0 & 2 + e \cos f \end{bmatrix} \right. \\ &\quad \left. + 2e \sin f \left(\frac{p^2}{h(1 + e \cos f)^2} - 1 \right) \begin{bmatrix} 0 & 2 & 0 \\ -2 & 0 & 0 \\ 0 & 0 & 0 \end{bmatrix} \right\}, \\ \tilde{\mathbf{G}}_{lerm} &= \begin{bmatrix} 0 & -2 & 0 \\ 2 & 0 & 0 \\ 0 & 0 & 0 \end{bmatrix}, \end{aligned} \quad (25)$$

the nonlinear controlled TH equations with control inputs $\tilde{\mathbf{u}}(\tilde{\mathbf{x}})$ are given by,

$$\begin{aligned} \frac{d^2}{df^2} \begin{bmatrix} \tilde{x} \\ \tilde{y} \\ \tilde{z} \end{bmatrix} &= -\tilde{\mathbf{K}}_{lerm} \begin{bmatrix} \tilde{x} \\ \tilde{y} \\ \tilde{z} \end{bmatrix} - \tilde{\mathbf{G}}_{lerm} \frac{d}{df} \begin{bmatrix} \tilde{x} \\ \tilde{y} \\ \tilde{z} \end{bmatrix} \\ &+ \frac{p^4}{h^2(1 + e \cos f)^3} \begin{bmatrix} \tilde{a}_{nx}(\tilde{x}, \tilde{y}, \tilde{z}) \\ \tilde{a}_{ny}(\tilde{x}, \tilde{y}, \tilde{z}) \\ \tilde{a}_{nz}(\tilde{x}, \tilde{y}, \tilde{z}) \end{bmatrix} + \tilde{\mathbf{u}}(\tilde{\mathbf{x}}), \end{aligned} \quad (26)$$

where \tilde{a}_n^* ($\tilde{x}, \tilde{y}, \tilde{z}$) are the perturbation accelerations expressed in terms of the scaled coordinates. Given a full state control input vector in the scaled TH frame as,

$$\tilde{\mathbf{u}}(\tilde{\mathbf{x}}) = -\tilde{\mathbf{K}}_f \tilde{\mathbf{x}} = -\tilde{\mathbf{K}}_f \begin{bmatrix} \tilde{x} & \tilde{y} & \tilde{z} & \frac{d\tilde{x}}{df} & \frac{d\tilde{y}}{df} & \frac{d\tilde{z}}{df} \end{bmatrix}^T, \tag{27}$$

since,

$$\tilde{\mathbf{x}} = \mathbf{T}\mathbf{x}, \quad \mathbf{T} = \begin{bmatrix} (1 + e \cos f) \mathbf{I} & \mathbf{0} \\ -(e \sin f) \mathbf{I} & \frac{p^2}{h(1 + e \cos f)} \mathbf{I} \end{bmatrix}, \tag{28}$$

the physical control input vector is,

$$\begin{aligned} \mathbf{u}(\mathbf{x}) &= \frac{h^2 (1 + e \cos f)^3}{p^4} \tilde{\mathbf{u}}(\mathbf{T}\mathbf{x}) = -\frac{h^2 (1 + e \cos f)^3}{p^4} \tilde{\mathbf{K}}_f \mathbf{T}\mathbf{x} \\ &= -\frac{h^2 (1 + e \cos f)^3}{p^4} \tilde{\mathbf{K}}_f \mathbf{T} \begin{bmatrix} x & y & z & \frac{dx}{df} & \frac{dy}{df} & \frac{dz}{df} \end{bmatrix}^T. \end{aligned} \tag{29}$$

Thus, in terms of the original state variables the physical control input vector is,

$$\mathbf{u}(\mathbf{x}) = -\mathbf{K}_f \mathbf{x} = -\mathbf{K}_f \begin{bmatrix} x & y & z & \frac{dx}{df} & \frac{dy}{df} & \frac{dz}{df} \end{bmatrix}^T, \tag{30}$$

with

$$\begin{aligned} \mathbf{K}_f &= -\frac{h^2 (1 + e \cos f)^3}{p^4} \tilde{\mathbf{K}}_f \mathbf{T} \\ &= -\frac{h^2 (1 + e \cos f)^3}{p^4} \tilde{\mathbf{K}}_f \begin{bmatrix} (1 + e \cos f) \mathbf{I} & \mathbf{0} \\ -(e \sin f) \mathbf{I} & \frac{p^2}{h(1 + e \cos f)} \mathbf{I} \end{bmatrix}. \end{aligned} \tag{31}$$

4. LINEAR QUADRATIC NONLINEAR GAUSSIAN (LQNG) DESIGN. The strategy adopted to design the controller is to adopt the methodology of the linear quadratic regulator for the synthesis of the control laws. To apply the methodology of the linear quadratic regulator, Equations (26) must first be linearized. To linearize Equations (26) the control input vector is expressed as, $\tilde{\mathbf{u}}(\tilde{\mathbf{x}}) = \tilde{\mathbf{u}}_0(\tilde{\mathbf{x}}) + \tilde{\mathbf{u}}_1(\tilde{\mathbf{x}})$. The control input $\tilde{\mathbf{u}}_0(\tilde{\mathbf{x}})$ is chosen in terms of $\hat{\tilde{x}}, \hat{\tilde{y}}$ and $\hat{\tilde{z}}$ which are estimates of \tilde{x}, \tilde{y} and \tilde{z} respectively as,

$$\tilde{\mathbf{u}}_0(\tilde{\mathbf{x}}) = -\frac{p^4}{h^2 (1 + e \cos f)^3} \begin{bmatrix} \tilde{a}_{nx} \left(\hat{\tilde{x}}, \hat{\tilde{y}}, \hat{\tilde{z}} \right) \\ \tilde{a}_{ny} \left(\hat{\tilde{x}}, \hat{\tilde{y}}, \hat{\tilde{z}} \right) \\ \tilde{a}_{nz} \left(\hat{\tilde{x}}, \hat{\tilde{y}}, \hat{\tilde{z}} \right) \end{bmatrix}, \tag{32}$$

Thus Equations (26) reduce to,

$$\frac{d^2}{df^2} \begin{bmatrix} \tilde{x} \\ \tilde{y} \\ \tilde{z} \end{bmatrix} = -\tilde{\mathbf{K}}_{Ierm} \begin{bmatrix} \tilde{x} \\ \tilde{y} \\ \tilde{z} \end{bmatrix} - \tilde{\mathbf{G}}_{Ierm} \frac{d}{df} \begin{bmatrix} \tilde{x} \\ \tilde{y} \\ \tilde{z} \end{bmatrix} + \frac{p^4}{h^2 (1 + e \cos f)^3} \begin{bmatrix} \tilde{a}_{nx}(\tilde{x}, \tilde{y}, \tilde{z}) - \tilde{a}_{nx}(\hat{\tilde{x}}, \hat{\tilde{y}}, \hat{\tilde{z}}) \\ \tilde{a}_{ny}(\tilde{x}, \tilde{y}, \tilde{z}) - \tilde{a}_{ny}(\hat{\tilde{x}}, \hat{\tilde{y}}, \hat{\tilde{z}}) \\ \tilde{a}_{nz}(\tilde{x}, \tilde{y}, \tilde{z}) - \tilde{a}_{nz}(\hat{\tilde{x}}, \hat{\tilde{y}}, \hat{\tilde{z}}) \end{bmatrix} + \tilde{\mathbf{u}}_1(\tilde{\mathbf{x}}). \quad (33)$$

The estimates of the perturbation accelerations components $\tilde{a}_{n*}(\hat{\tilde{x}}, \hat{\tilde{y}}, \hat{\tilde{z}})$ are evaluated at the mid-point of the current integration step. Thus, the right-hand side of Equation (33) represents the error in the actual and estimated perturbation accelerations, which can be assumed to be a disturbance vector and ignored for purposes of designing the control input $\tilde{\mathbf{u}}_1(\tilde{\mathbf{x}})$.

However, it is often not possible to measure all the states of the system, which is in reality a nonlinear system. Moreover, the measurements are almost always noisy. For this reason, we adopt a nonlinear estimation methodology to reconstruct all the states from the measurements. The nonlinear estimation methodology is based on the unscented Kalman filter. Because the equations of motion are nonlinear, the separation theorem, which is often adopted to justify the independent design of the control laws and the solution of the state estimation problem, is no longer valid. Nevertheless, we will design the control input $\tilde{\mathbf{u}}_1(\tilde{\mathbf{x}})$ based on the linearized true anomaly-dependent discretized equations for the relative motion and implement these inputs by feeding back the estimates of the states rather than the original states of the system.

5. THE LINEAR TH EQUATIONS AND THEIR DISCRETIZATION. The linearized TH equations in the presence of control accelerations are given by,

$$\frac{d^2}{df^2} \begin{bmatrix} \tilde{x} \\ \tilde{y} \\ \tilde{z} \end{bmatrix} = -\tilde{\mathbf{K}}_{Ierm} \begin{bmatrix} \tilde{x} \\ \tilde{y} \\ \tilde{z} \end{bmatrix} - \tilde{\mathbf{G}}_{Ierm} \frac{d}{df} \begin{bmatrix} \tilde{x} \\ \tilde{y} \\ \tilde{z} \end{bmatrix} + \begin{bmatrix} 1 & 0 & 0 \\ 0 & 1 & 0 \\ 0 & 0 & 1 \end{bmatrix} \begin{bmatrix} \tilde{u}_{1x} \\ \tilde{u}_{1y} \\ \tilde{u}_{1z} \end{bmatrix}. \quad (34)$$

Equations (33) may be expressed as a set of first order equations in matrix form with the true anomaly as the independent variable,

$$\frac{d}{df} \tilde{\mathbf{x}} = \mathbf{A}(f) \tilde{\mathbf{x}} + [\mathbf{0} \quad \mathbf{I}]^T \tilde{\mathbf{u}}_1, \quad (35a)$$

with,

$$\mathbf{A}(f) \equiv \begin{bmatrix} \mathbf{0} & \mathbf{I} \\ -\tilde{\mathbf{K}}_{Ierm} & -\tilde{\mathbf{G}}_{Ierm} \end{bmatrix}. \quad (35b)$$

The coefficients of the equation are periodic with a period $T = 2\pi$. Thus, there exists a non-singular matrix $\mathbf{P}(f)$, periodic with period $T = 2\pi$ with $\mathbf{P}(0) = \mathbf{I}$, such that the

Table 1. Orbital elements defining the initial position of the Primary Satellite and orbiting body.

	a	e	i	Ω	ω	M
Satellite	7555.5km	0.0096	0.9575°	0°	90°	0°
Orbiting body	7555.5km	0.0096	0.9575°	0.00001°	90°	0°

change of the variables $\tilde{\mathbf{x}} = \mathbf{P}(f) \mathbf{z}$, transforms the system into a linear system with constant coefficients. The Floquet transition matrix which is also known as the monodromy matrix $\Phi(f, 0)$, which determines the stability of the system with $f = T$, satisfies,

$$\frac{d}{df} \Phi(f, 0) = \mathbf{A}(f) \Phi(f, 0), \quad \Phi(0, 0) = \mathbf{I}. \tag{36}$$

The solution $\tilde{\mathbf{x}}(f)$ then satisfies,

$$\tilde{\mathbf{x}}(f) = \Phi(f, 0) \tilde{\mathbf{x}}(0) + \int_0^f \Phi(f, \varphi) [\mathbf{0} \quad \mathbf{I}]^T \tilde{\mathbf{u}}_1 d\varphi, \tag{37}$$

which can also be expressed as,

$$\tilde{\mathbf{x}}(f + \Delta f) = \Phi(f + \Delta f, f) \tilde{\mathbf{x}}(f) + \int_0^{\Delta f} \Phi(f + \Delta f, f + \varphi) [\mathbf{0} \quad \mathbf{I}]^T \tilde{\mathbf{u}}_1(f + \varphi) d\varphi. \tag{38}$$

Assuming that the control input could be approximated as a constant over each integration interval and given by $\tilde{\mathbf{u}} = \tilde{\mathbf{u}}_1$, we have the discrete system,

$$\tilde{\mathbf{x}}(f + \Delta f) = \Phi(f + \Delta f, f) \tilde{\mathbf{x}}(f) + \Psi(f + \Delta f, f) \tilde{\mathbf{u}}(f), \tag{39}$$

with,

$$\Psi(f + \Delta f, f) = \int_0^{\Delta f} \Phi(f + \Delta f, f + \varphi) [\mathbf{0} \quad \mathbf{I}]^T d\varphi. \tag{40}$$

The discrete system given by Equation (39) may be expressed as,

$$\tilde{\mathbf{x}}(k + 1) = \tilde{\mathbf{A}}(k) \tilde{\mathbf{x}}(k) + \tilde{\mathbf{B}}(k) \tilde{\mathbf{u}}(k). \tag{41}$$

Equation (41) may be used to synthesise an optimal control law.

6. LINEAR QUADRATIC REGULATOR DESIGN. The design process for the discrete-time Linear Quadratic Regulator (LQR) with a finite final time when magnitude constraints are imposed on the state and control variables is discussed in this section. A finite final time quadratic performance index could be used, so the \mathbf{Q} and \mathbf{R} weighting

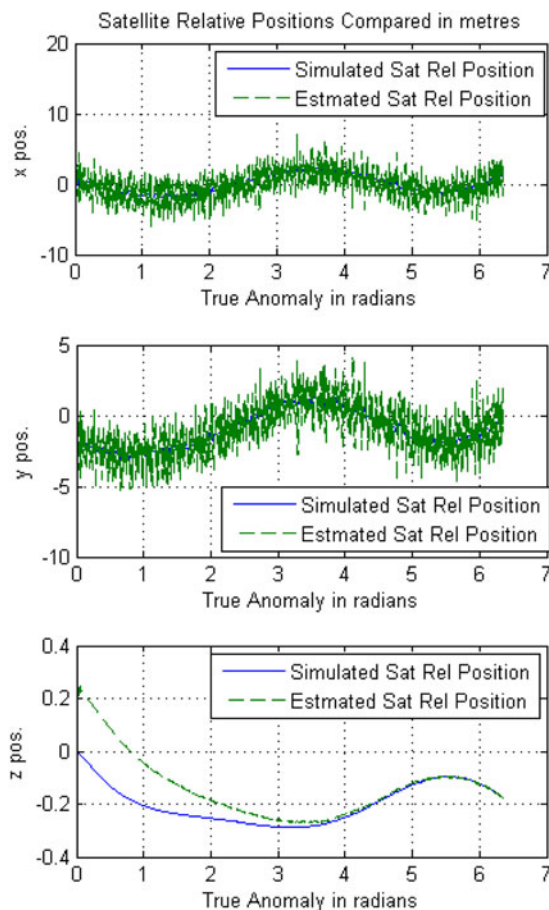


Figure 1. The simulated and estimated $[x \ y \ z]$ position coordinates of the primary satellite, relative to the secondary orbiting body in the closed loop case with the optimal control law.

matrices will have to be chosen and an algebraic Riccati equation must be solved. In the absence of terminal constraints, the performance index is of the form:

$$J = \frac{1}{2} \sum_{k=0}^{N-1} (\tilde{\mathbf{x}}_k^T \mathbf{Q} \tilde{\mathbf{x}}_k + \tilde{\mathbf{u}}_k^T \mathbf{R} \tilde{\mathbf{u}}_k). \quad (42)$$

When a spacecraft is actuated upon by thrusters, the thrusts generated are small. Typically, a thruster generates thrusts from 1-2 N. Thus, it is essential that in the design of the control laws the elements of the matrix \mathbf{R} are of the order of 10^1 or more. During a controlled rendezvous the position coordinates are reduced from 10-100 m to less than a millimetre. Thus, the elements of the matrix \mathbf{Q} are of the order of 10^5 or less. An iterative process is used to update the weighting matrices used in the performance index to meet the terminal constraints. An alternate but equivalent approach is to use the Model Predictive Control (MPC) approach. To briefly describe the synthesis of linear optimal control based

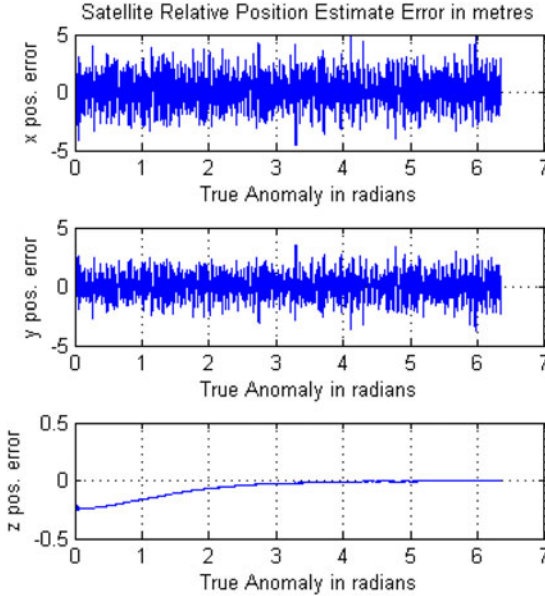


Figure 2. The errors in the simulated and estimated $[x \ y \ z]$ position coordinates of the primary satellite, relative to the secondary orbiting body.

on the MPC approach, consider a linear discrete time system in the form,

$$\mathbf{x}(k + 1) = \mathbf{A}(k) \mathbf{x}(k) + \mathbf{B}(k) \mathbf{u}(k), \quad \mathbf{y}(k) = \mathbf{C}(k) \mathbf{x}(k). \tag{43}$$

Our aim is to find an optimal control input sequence defined over a control prediction window, $\mathbf{u}(j), j = 0, 1, 2 \dots N - 1$ or the vector $\mathbf{U} = [\mathbf{u}^T(0) \ \mathbf{u}^T(1) \ \dots \ \mathbf{u}^T(N - 1)]^T$ so as to minimise the performance index, which now includes a terminal weighting matrix \mathbf{Q}_N ,

$$J(\mathbf{x}(0), \mathbf{U}) = \sum_{k=0}^{N-1} \{ \mathbf{y}^T(k) q \mathbf{Q} \mathbf{y}(k) + \mathbf{u}^T(k) r \mathbf{R} \mathbf{u}(k) \} + \mathbf{y}^T(N) q \mathbf{Q}_N \mathbf{y}(N), \tag{44}$$

where q and r are scalar scaling parameters which are used to re-scale the relative contributions of the states and the control inputs to the cost function. When the magnitude of the control input is relatively large when compared with the magnitude of the state, r is assumed to be a small number relative to q and vice-versa.

Defining the vector, $\mathbf{X} = [\mathbf{x}^T(1) \ \mathbf{x}^T(2) \ \dots \ \mathbf{x}^T(N - 1) \ \mathbf{x}^T(N)]$, we may write,

$$J(\mathbf{x}(0), \mathbf{U}) = q \mathbf{x}^T(0) \mathbf{C}^T(0) \mathbf{Q} \mathbf{C}(0) \mathbf{x}(0) + q \mathbf{X}^T \bar{\mathbf{Q}} \mathbf{X} + r \mathbf{U}^T \bar{\mathbf{R}} \mathbf{U}, \tag{45}$$

where $\bar{\mathbf{Q}}$ is a block diagonal matrix with matrix $\mathbf{C}^T(k) \mathbf{Q} \mathbf{C}(k), k = 1, 2 \dots N - 1$ along the diagonal except the last element which is $\mathbf{C}^T(N) \mathbf{Q}_N \mathbf{C}(N)$; $\bar{\mathbf{R}}$ is a block diagonal matrix with matrix \mathbf{R} along the diagonal. Using the state space model Equation (43) recursively,

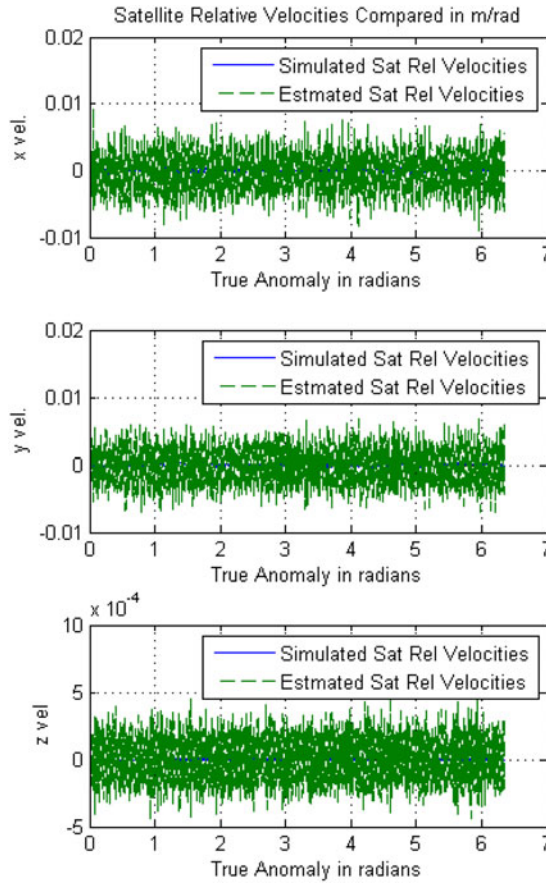


Figure 3. The simulated and estimated $[x \ y \ z]$ velocity components of the primary satellite, relative to the secondary orbiting body in the closed loop case.

we may construct a prediction model in the form,

$$\mathbf{X} = \mathbf{S}\mathbf{U} + \mathbf{T}\mathbf{x}(0) \tag{46}$$

where

$$\mathbf{S} = \begin{bmatrix} \mathbf{B} & \mathbf{0} & \mathbf{0} & \mathbf{0} \\ \mathbf{A}(1)\mathbf{B} & \mathbf{B} & \mathbf{0} & \mathbf{0} \\ \dots & \dots & \dots & \dots \\ \left(\prod_{k=N-1}^1 \mathbf{A}(k)\right)\mathbf{B} & \left(\prod_{k=N-2}^1 \mathbf{A}(k)\right)\mathbf{B} & \dots & \mathbf{B} \end{bmatrix}, \mathbf{T} = \begin{bmatrix} \mathbf{A}(0) \\ \mathbf{A}(1)\mathbf{A}(0) \\ \dots \\ \prod_{k=N-1}^0 \mathbf{A}(k) \end{bmatrix}. \tag{47}$$

We have assumed for simplicity that \mathbf{B} is constant but not \mathbf{A} . The above formula could be generalised for the case when \mathbf{B} is not constant. Thus, the cost function may be expressed as,

$$J(\mathbf{x}(0), \mathbf{U}) = \frac{1}{2}\mathbf{x}(0)^T \mathbf{G}\mathbf{x}(0) + \frac{1}{2}\mathbf{U}^T \mathbf{H}\mathbf{U} + \mathbf{x}^T(0) \mathbf{F}\mathbf{U}, \tag{48}$$

with, $\mathbf{G} = 2q(\mathbf{T}^T \bar{\mathbf{Q}}\mathbf{T} + \mathbf{C}^T(0)\mathbf{Q}\mathbf{C}(0))$, $\mathbf{H} = 2r\bar{\mathbf{R}} + 2q\mathbf{S}^T \bar{\mathbf{Q}}\mathbf{S}$ and $\mathbf{F} = q\mathbf{T}^T \bar{\mathbf{Q}}\mathbf{S}$.

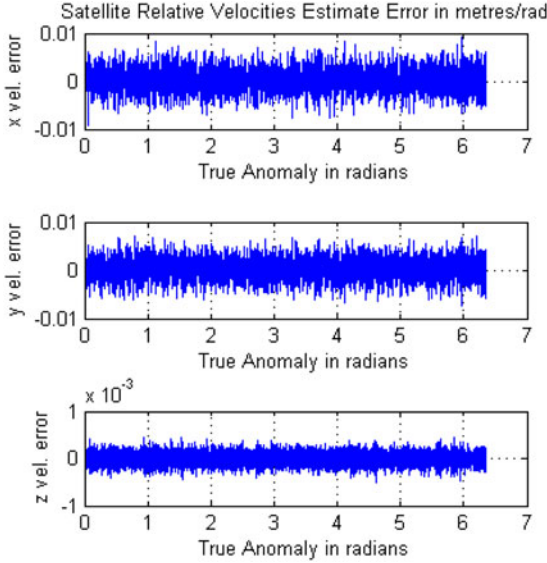


Figure 4. The errors in the simulated and estimated $[x \ y \ z]$ velocity components of the primary satellite, relative to the secondary orbiting body.

The optimum control sequence is obtained by setting the gradient of $J(\mathbf{x}(0), \mathbf{U})$ to zero. Minimising the cost function results in,

$$\begin{aligned} dJ(\mathbf{x}(0), \mathbf{U}) / d\mathbf{U} = \mathbf{U}^T \mathbf{H} + \mathbf{x}^T(0) \mathbf{F} = 0 &\Rightarrow \mathbf{H}\mathbf{U} + \mathbf{F}^T \mathbf{x}(0) = 0 \Rightarrow \mathbf{U} \\ &= -\mathbf{H}^{-1} \mathbf{F}^T \mathbf{x}(0). \end{aligned} \tag{49}$$

The state $\mathbf{x}(0)$, at the start of the prediction window, is assumed to represent the state at the next time instant, in real time. The control law based on the receding horizon is,

$$\mathbf{u}(k) = -[1 \ 0 \ \dots \ 0] \mathbf{H}^{-1} \mathbf{F}^T \mathbf{x}(k). \tag{50}$$

The control sequence is recursively calculated over successive control prediction windows. The product $\mathbf{H}^{-1} \mathbf{F}^T$ may be expressed as

$$\mathbf{H}^{-1} \mathbf{F}^T = \frac{q}{2} (r\bar{\mathbf{R}} + q\mathbf{S}^T \bar{\mathbf{Q}}\mathbf{S})^{-1} \mathbf{S}^T \bar{\mathbf{Q}}\mathbf{T} = \frac{q^2}{2} \left(\frac{r}{q} \bar{\mathbf{R}} + q\mathbf{S}^T \bar{\mathbf{Q}}\mathbf{S} \right)^{-1} \mathbf{S}^T \bar{\mathbf{Q}}\mathbf{T}. \tag{51}$$

If we let $q = 1$, Equation (51) reduces to,

$$\mathbf{H}^{-1} \mathbf{F}^T = \frac{1}{2} (r\bar{\mathbf{R}} + \mathbf{S}^T \bar{\mathbf{Q}}\mathbf{S})^{-1} \mathbf{S}^T \bar{\mathbf{Q}}\mathbf{T}, \tag{52}$$

where r is treated as a free parameter to be chosen.

7. THE UNSCENTED KALMAN FILTER. The basic unscented Kalman filter is identical to the filter implemented in Vepa and Amzhari (2011) and Vepa (2017) which is briefly summarised in the following.

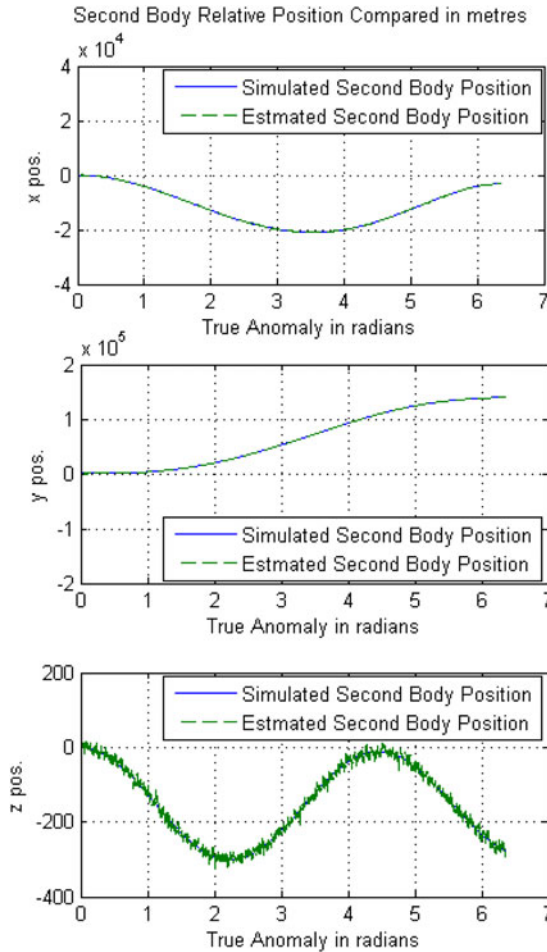


Figure 5. The simulated and estimated $[x \ y \ z]$ position coordinates of the secondary orbiting body relative to the position of a notional particle in a Keplerian orbit.

Consider a random variable \mathbf{w} with dimension L which is going through the nonlinear transformation, $\mathbf{y} = \mathbf{f}(\mathbf{w})$. The initial conditions are that \mathbf{w} has a mean $\bar{\mathbf{w}}$ and a covariance $\mathbf{P}_{\mathbf{w}\mathbf{w}}$. To calculate the statistics of \mathbf{y} , a matrix χ of $2L + 1$ sigma vectors is formed. We have chosen to use the scaled unscented transformation proposed by Julier (2002), as this transformation gives the added flexibility of scaling the sigma points to ensure that the covariance matrices are always positive definite.

Given a general discrete-time nonlinear dynamic system in the form,

$$\mathbf{x}_{k+1} = \mathbf{f}_k(\mathbf{x}_k, \mathbf{u}_k) + \mathbf{w}_k, \quad \mathbf{y}_k = \mathbf{h}_k(\mathbf{x}_k) + \mathbf{v}_k \tag{53}$$

where $\mathbf{x}_k \in R^n$ is the state vector, $\mathbf{u}_k \in R^r$ is the known input vector, $\mathbf{y}_k \in R^m$ is the output vector at time k . \mathbf{w}_k and \mathbf{v}_k are, respectively, the disturbance or process noise and sensor noise vectors, which are assumed to be Gaussian white noise with zero mean. Furthermore \mathbf{Q}_k and \mathbf{R}_k are assumed to be the covariance matrices of the process noise sequence, \mathbf{w}_k

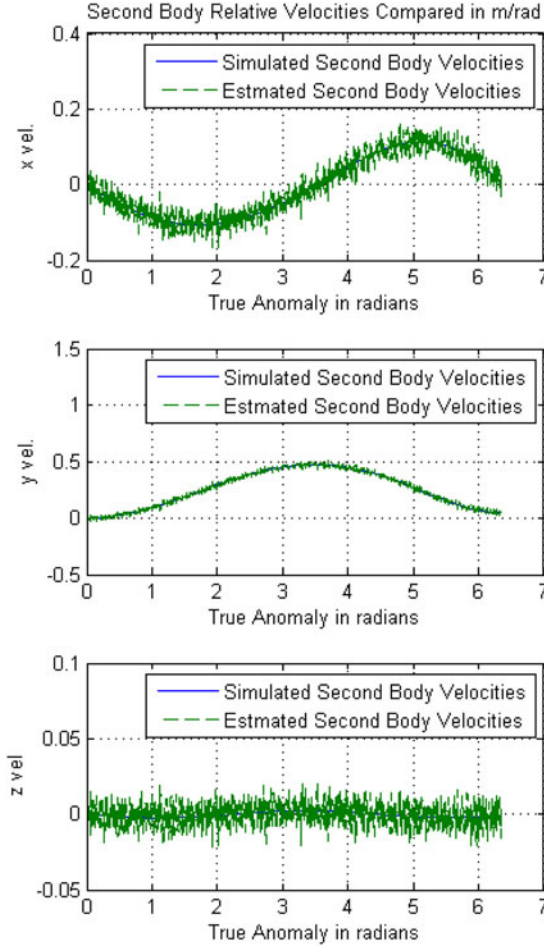


Figure 6. The simulated and estimated $[x \ y \ z]$ velocity components of the secondary orbiting body relative to the position of a notional particle in a Keplerian orbit.

and the measurement noise sequence, \mathbf{v}_k respectively. The unscented transformations of the states corresponding to the functions $\mathbf{f}_k(\mathbf{x}_k, \mathbf{u}_k)$ and $\mathbf{h}_k(\mathbf{x}_k)$ are denoted respectively as,

$$\mathbf{f}_k^{UT} = \mathbf{f}_k^{UT}(\mathbf{x}_k, \mathbf{u}_k), \quad \mathbf{h}_k^{UT} = \mathbf{h}_k^{UT}(\mathbf{x}_k) \tag{54}$$

while the transformed covariance matrices and cross-covariance are respectively denoted as,

$$\mathbf{P}_k^{ff} = \mathbf{P}_k^{ff}(\hat{\mathbf{x}}_k, \mathbf{u}_k), \quad \mathbf{P}_k^{hh} = \mathbf{P}_k^{hh}(\hat{\mathbf{x}}_k^-) \text{ and } \mathbf{P}_k^{xh} = \mathbf{P}_k^{xh}(\hat{\mathbf{x}}_k^-, \mathbf{u}_k). \tag{55}$$

The UKF estimator can then be expressed in a compact form. The state time-update equation, the propagated covariance, the Kalman gain \mathbf{K}_k , the state estimate $\hat{\mathbf{x}}_k$ and the

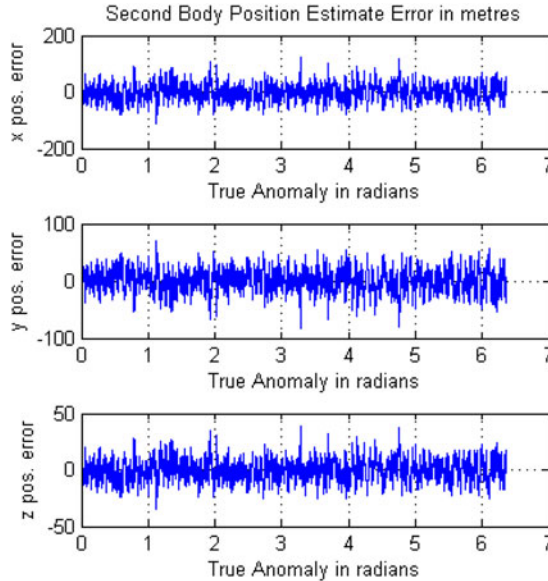


Figure 7. Errors in the simulated and estimated $[x \ y \ z]$ position coordinates of the secondary orbiting body relative to the position of a notional particle in a Keplerian orbit.

updated covariance $\hat{\mathbf{P}}_k$ are respectively given by,

$$\hat{\mathbf{x}}_k^- = \mathbf{f}_{k-1}^{UT} (\hat{\mathbf{x}}_{k-1}) \quad (56a)$$

$$\hat{\mathbf{P}}_k^- = \mathbf{P}_{k-1}^{ff} + \mathbf{Q}_{k-1} \quad (56b)$$

$$\mathbf{K}_k = \hat{\mathbf{P}}_k^{xh-} \left(\hat{\mathbf{P}}_k^{hh-} + \mathbf{R}_k \right)^{-1} \quad (56c)$$

$$\hat{\mathbf{x}}_k = \hat{\mathbf{x}}_k^- + \mathbf{K}_k [\mathbf{z}_k - \mathbf{h}_k^{UT} (\hat{\mathbf{x}}_k^-)] \quad (56d)$$

$$\hat{\mathbf{P}}_k = \hat{\mathbf{P}}_k^- - \mathbf{K}_k \left(\hat{\mathbf{P}}_k^{hh-} + \mathbf{R}_k \right)^{-1} \mathbf{K}_k^T. \quad (56e)$$

Equations (56a)-(56e) are in the same form as the traditional Kalman filter and the extended Kalman filter. Thus, higher order non-linear models capturing significant aspects of the dynamics may be employed to ensure that the Kalman filter algorithm can be implemented to effectively estimate the states in practice. The control input $\tilde{\mathbf{u}}_1(\tilde{\mathbf{x}})$ is assumed to be given by,

$$\tilde{\mathbf{u}}_1(\tilde{\mathbf{x}}) = \tilde{\mathbf{u}}(k) = - [1 \ 0 \ \dots \ 0] \mathbf{H}^{-1} \mathbf{F}^T \hat{\tilde{\mathbf{x}}}(k), \quad (57)$$

where the vector $\hat{\tilde{\mathbf{x}}}$ is an estimate of the vector $\tilde{\mathbf{x}}$ obtained by the unscented Kalman filter.

8. TYPICAL SIMULATIONS AND RESULTS. The initial position and velocity of the primary satellite are obtained from the initial classical orbital elements defined in Table 1. From these orbital elements, the initial position and velocity vector of the satellite are obtained. The actual initial location of the secondary orbiting body is defined by the orbital

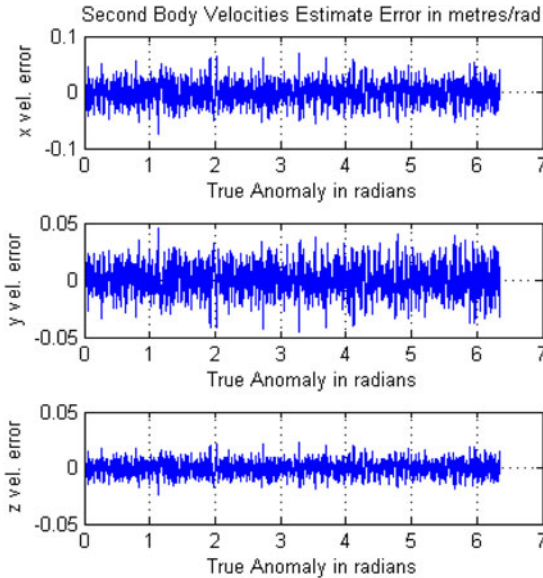


Figure 8. Errors in the simulated and estimated $[x \ y \ z]$ velocity components of the secondary orbiting body relative to the position of a notional particle in a Keplerian orbit.

elements set shown in Table 1 and converted to position and velocity vectors relative to the satellite. The orbital elements defining the reference Keplerian orbit are identical to the primary satellite's initial orbital elements.

In all three cases the size and shape of the orbital ellipse and the inclination of the orbit plane are assumed to be the same. Only the argument of the ascending node (Ω) is assumed to be different by 0.00001° . From the orbital elements, the initial position and velocity of the secondary orbiting body are defined relative to the satellite. The numerical integration was performed using the Runge-Kutta Dormand-Prince 4(5) (Dormand and Prince, 1980). The overall prediction and estimation window is in excess of 2π radians which is covered in 7,500 integration steps. The non-dimensionalising distance was chosen to be $r_{sc} = 35,786$ km, which is the radius of the geostationary orbit, and the unit of time was $t_{sc} = 86,400$ sec or a day. The position coordinates used for integration are the scaled TH coordinates. All the results are plotted in SI units.

A total of 13 noisy measurements are made: a pair of angles that the satellite makes with the Sun, and another pair with the Moon, the satellite's distance vector from the Earth which is assumed to be relatively very noisy or uncertain and the satellite's relative position and velocity vectors relative to the secondary orbiting body. The positions of the Sun and Moon are assumed to be known from the relevant ephemeris and obtained in the same manner as in Vepa (2017).

Figure 1 presents the simulated and estimated position coordinates of the primary satellite, relative to the secondary orbiting body in the closed loop case, which are compared. The errors in the relative position coordinate estimates, relative to the secondary orbiting body are shown in Figure 2. Figure 3 presents the corresponding simulated and estimated velocity components of the satellite relative to the secondary orbiting body in the closed loop case, which are compared against each other. The errors in these relative velocity

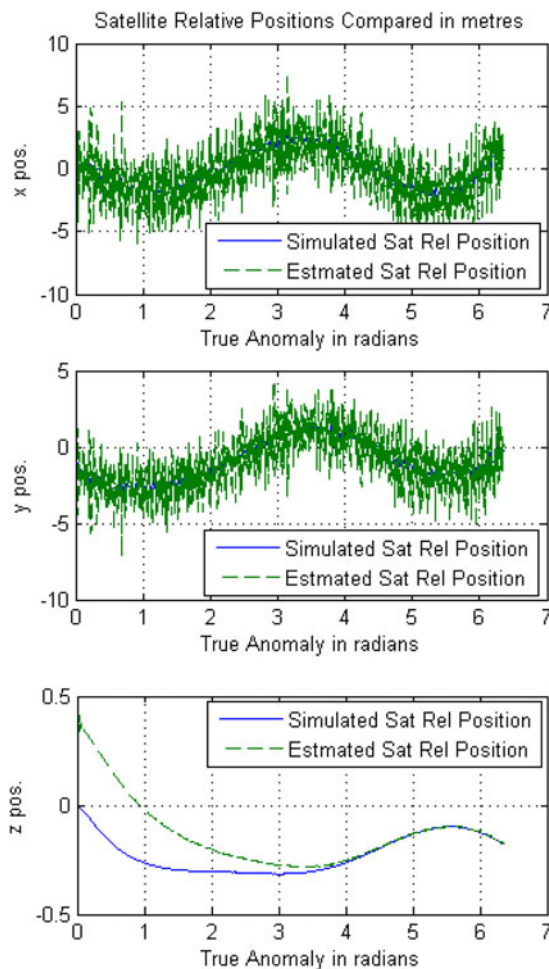


Figure 9. The simulated and estimated $[x \ y \ z]$ position coordinates of the primary satellite, relative to the secondary orbiting body with the additional integral term in the control law.

components are shown in Figure 4. The control laws were evaluated both by applying the discrete linear quadratic regulator algorithm (with an infinite horizon) at every true anomaly step as well as by the MPC algorithm over a finite control prediction horizon. The results in both cases were quite similar and for this reason only the latter results are presented here.

Figures 5 and 6 show the estimates of the second body position and velocity in the TH coordinates, relative to a particle in a notional Keplerian orbit. Figures 7 and 8 show the corresponding errors in the estimates of the second body position and velocity. Although these errors are an order of magnitude greater than the errors in the satellites' relative position and velocity estimates they are still less than 0.16% of the secondary orbiting body's absolute position and velocity component magnitudes relative to the Earth's centre.

Examining the results in Figure 1 closely it is clear that there is an accumulation of position error in the radial direction which approaches 4 m and that the satellite is falling behind

in its pursuit of the secondary orbiting object. Moreover, the response resembles the typical response of a first order system to a step input as the error between the pursuer, the primary satellite, and the secondary orbiting body approaches a steady state value, albeit slowly, over one orbit. This is a classic case that demands from a practical standpoint the use of integral control to drive the position error, due to the residual disturbance acceleration, to zero. The control is now assumed to be,

$$\tilde{\mathbf{u}}_1(\tilde{\mathbf{x}}) = \bar{\mathbf{u}}(k) + K_I \sum_{j=1}^{k-1} \bar{\mathbf{u}}(j) \Delta f, \quad (58)$$

where the integral matrix gain K_I is nominally chosen to be equal to,

$$K_I = \begin{bmatrix} 2 & 0 & 0 \\ 0 & 0.5 & 0 \\ 0 & 0 & 0 \end{bmatrix}, \quad (59)$$

Δf is the integration step in terms of the true anomaly and $\bar{\mathbf{u}}(k)$ is the previously designed optimal control law.

The results corresponding to [Figure 1](#), with the additional term representing integral control in the control law defined in Equation (58), are shown in [Figure 9](#). There is now a significant reduction in the position error of the pursuer, the primary satellite, relative to the secondary orbiting body which approaches an almost steady state value after one orbit. The position error components are well below 4 m and decreasing over one orbit. The relative positions and relative velocities are within acceptable limits and rendezvous could be established as soon as the error components are near zero and attitude synchronisation is achieved.

9. CONCLUSIONS. One of the most significant features of this work is the fact that the integration steps in terms of true anomaly needed to be much smaller than the equivalent time domain integration in order to obtain state estimates with similar error bounds. On the other hand, a significant benefit in using nonlinear true anomaly varying TH equations was the ease with which the feedback controller was synthesised. Thus, the disadvantages encountered in solving the estimation problem are more than compensated by the advantages in solving the control problem.

In this paper, we have quite clearly demonstrated the application of the nonlinear true anomaly-varying TH equations to the problem of state estimation and control of a satellite chasing a secondary orbiting body and seeking to rendezvous with it without any assistance from it. We have also demonstrated the application of the UKF to the problem of state estimation using the nonlinear TH equations as well as the use of integral control to establish a practically feasible control law. We have also shown the systematic derivation of the nonlinear, controlled TH equations in the presence of perturbing accelerations. Final rendezvous and docking or berthing can only be achieved following the attitude synchronisation of the pursuer satellite with the target body. Estimation and control of the relative attitude is a problem that also needs to be addressed and it will be published independently. There are several practical applications to this work, particularly if one wishes to design autonomous space vehicles capable of catching up with a secondary orbiting body.

REFERENCES

- Capó-Lugo, P.A. and Bainum, P.M. (2011). Formation flying control implementation for highly elliptical orbits. *Journal of Aerospace Engineering, Sciences and Applications*, **III**(1), 1–18.
- Capó-Lugo, P.A. and Bainum, P.M. (2007). Active control schemes based on the linearized Tschauner–Hempel equations to maintain the separation distance constraints for the NASA benchmark tetrahedron constellation. *Journal of Mechanics of Materials and Structures*, **2**(8), 1541–1559.
- Cho, H. and Udwarda, F.E. (2010). Explicit solution to the full nonlinear problem for satellite formation-keeping. *Acta Astronautica*, **67**, 369–387.
- Clohessy, W.H. and Wiltshire, R.S. (1960). Terminal Guidance System for Satellite Rendezvous. *Journal of Guidance, Control, and Dynamics*, **27**(13), 653–658.
- Condurache, D. (2012). Spacecraft Relative Orbital Motion, Chapter 3, in *Advances in Spacecraft Systems and Orbit Determination*, Ed. Ghadawala, R., INTECH, DOI: 10.5772/2408.
- Coverstone-Carroll, V. and Trussing, J.E. (1993). Optimal cooperative power limited rendezvous between neighbouring circular orbits. *Journal of Guidance, Control, and Dynamics*, **16**(8), 1045–1054.
- Cui, N.G., Zhou, B. and Duan, G.R. (2011). Output feedback elliptical orbital rendezvous via state-dependent Riccati differential equations. *IET Control Theory & Applications*, **7**(14), 1429–1436.
- Dormand, J.R. and Prince, P.J. (1980). A family of embedded Runge-Kutta formulae, *Journal of Computational and Applied Mathematics*, **6**, 19–26.
- Dwidar, H.R. and Owis, A.H. (2013). Relative Motion of Formation Flying with Elliptical Reference Orbit, *International Journal of Advanced Research in Artificial Intelligence*, **2**(8), 79–86.
- Felisiak, P. (2015). Control of Spacecraft for Rendezvous Maneuver in an Elliptical Orbit, PhD Thesis, Department of Cryogenic, Aviation and Process Engineering, Wrocław University of Technology, Wrocław, Poland.
- Hartley, E.N., Gallieri, M., and Maciejowski, J.M. (2013). Terminal spacecraft rendezvous and capture using LASSO MPC, *International Journal of Control*, **86**(15), 2104–2113.
- Hill, G.W. (1878). Researches in the Lunar Theory. *American Journal of Mathematics*, **23**(1), 5–26.
- Julier, S.J. (2002). The Scaled Unscented Transformation. *Proceedings of the American Control Conference*, **6**, 4555–4559.
- Leomanni, M., Rogers, E. and Gabriel, S.B. (2014). Explicit model predictive control approach for low-thrust spacecraft proximity operations, *Journal of Guidance, Control, and Dynamics*, **37**(8), 1780–1790.
- NASA (2011). *History of Space Shuttle Rendezvous*, JSC – 63400, Revision 3, Mission Operations Directorate, Flight Dynamics Division, NASA Lyndon B. Johnson Space Center, Houston, Texas, USA.
- Nicholas, A.K. (2013). Attitude and Formation Control Design and System Simulation for a Three-Satellite CubeSat Mission, Master of Science Thesis (Adviser Miller D.W.), Department of Aeronautics and Astronautics, Massachusetts Institute of Technology.
- Palacios, L., Ceriotti, M. and Radice, G. (2013). Autonomous distributed LQR/APF control algorithms for CubeSat swarms manoeuvring in eccentric orbits. In: *64th International Astronautical Congress (IAC)*, 23–27 Sep 2013, Beijing, China.
- Perez, A.C. (2017). Applications of Relative Motion Models Using Curvilinear Coordinate Frames, PhD Thesis, Utah State University, Logan, Utah.
- Tschauner, J. and Hempel, P. (1965). Rendezvous with a target describing an elliptical trajectory (In German). *Astronautica Acta*, **11**(2), 104–109.
- Vepa, R. (2017). Joint Position Localisation of Spacecraft and Debris for Autonomous Navigation Applications using Angle Measurements only. *The Journal of Navigation*, **70**(4), 748–760.
- Vepa, R. and Zhahir, A. (2011). High-Precision Kinematic Satellite and Doppler Aided Inertial Navigation System. *The Journal of Navigation*, **64**(01), 91–108.
- Weiss, A., Baldwin, M., Erwin, R.S., and Kolmanovsky, I. (2015). Model predictive control for spacecraft rendezvous and docking: Strategies for handling constraints and case studies. *IEEE Transactions on Control Systems Technology*, **23**(4), 1638–1647.
- Yao, Y., Xie, R. and He, F. (2010). Flyaround Orbit Design for Autonomous Rendezvous Based on Relative Orbit Elements. *Journal of Guidance, Control, and Dynamics*, **33**(7), 1687–1692.
- Yazhong, L., Jin, Z. and Guojin, T. (2014). Survey of orbital dynamics and control of space rendezvous. *Chinese Journal of Aeronautics*, **27**(1), 1–11.